Sawtooth Control in JET with ITER relevant low field side resonance ICRH and ITER like wall

J. P. Graves[1], M. Lennholm[2], I. T. Chapman[3], E. Lerche[4], M. Reich[5], B. Alper[3], V. Bobkov[5], R. Dumont[6], J. M. Faustin[1], P. Jacquet[3], F. Jaulmes[7], T. Johnson[8], D. L. Keeling[3], Yueqiang Liu[3], T. Nicolas[6], S. Tholerus[8], T. Blackman[3], I. S. Carvalho[9], R. Coelho[9], D. Van Eester[4], R. Felton[3], M. Goniche[6], V. Kiptily[3], I. Monakhov[3], M. F. F. Nave[9], C. Perez von Thun[10], R. Sabot[6], C. Sozzi[11], M. Tsalas[7] and JET EFDA Contributors*

JET-EFDA, Culham Science Centre, OX14 3DB, Abingdon, UK

[1] *École Polytechnique Fédérale de Lausanne (EPFL), Centre de Recherches en Physique des Plasmas (CRPP), 1015 Lausanne, Switzerland*

[2] *EFDA-JET CSU, Culham Science Centre, Abingdon, OX14 3DB, UK*

[3] *CCFE Fusion Association, Culham Science Centre, Abingdon, UK*

[4] *LPP-ERM/KMS, TEC Partner, Brussels, Belgium*

[5] *Max-Planck-Institut für Plasma Physik, Boltzmannstr. 2, 85748 Garching, Germany*

[6] *CEA-Cadarache, F-13108 St. Paul lez Durance, France*

[7] *FOM Institute DIFFER Dutch Institute For Fundamental Energy Research, FOM, Nieuwegein, The Netherlands*

[8] *Association VR, KTH, SE-100 44 Stockholm, Sweden*

[9] *Instituto de Plasmas e Fusão Nuclear, Instituto Superior Técnico, Universidade de Lisboa, P-1049-001, Lisboa, Portugal*

[10] *University of Innsbruck, Österreichische Akademie der Wissenshaften (ÖAW), Austria and*

[11] *Isituto di Fisica del Plasma CNR, 20125 Milano, Italy*

New experiments at JET with the ITER like wall show for the first time that ITER-relevant low field side resonance first harmonic ICRH with can be used to control sawteeth that have been initially lengthened by fast particles. In contrast to previous [J. P. Graves *et al*, Nature Communs **3**, 624 (2012)] high field side resonance sawtooth control experiments undertaken at JET, it is found that the sawteeth of L-mode plasmas can be controlled with less accurate alignment between the resonance layer and the sawtooth inversion radius. This advantage, as well as the discovery that sawteeth can be shortened with various antenna phasings, including dipole, indicates that ICRH is a particularly effective and versatile tool that can be used in future fusion machines for controlling sawteeth. Without sawtooth control, NTMs and locked modes were triggered at very low normalised beta. High power H-mode experiments show the extent to which ICRH can be tuned to control sawteeth and NTMs while simultaneously providing effective electron heating with improved flushing of high Z core impurities. Dedicated ICRH simulations using SELFO, SCENIC and EVE, including wide drift orbit effects, explain why sawtooth control is effective with various antenna phasings, and show that the sawtooth control mechanism cannot be explained by enhancement of the magnetic shear. Hybrid kinetic-MHD stability calculations using MISHKA and HAGIS unravel the optimal sawtooth control regimes in these ITER relevant plasma conditions.

PACS numbers: 52.55.Fa, 52.55Tn, 52.50Qt, 52.25.Pi, 52.35.Py

I. INTRODUCTION

The stabilising role of trapped alpha particles are expected to cause long sawtooth periods in ITER. Without adequate sawtooth control techniques, long sawteeth are predicted [1] to trigger fast growing neoclassical tearing modes (NTMs) during standard H-mode operation. Experiments at JET [2, 3] have shown that long period sawteeth can trigger NTMs deeply in L-mode when the normalised beta is only around $\beta_N = 0.8$, a value around half that expected during standard baseline ITER operation. NTMs could be avoided in these experiments by controlling sawteeth with ICRH resonance close to the $q = 1$ surface on the high field side, and the control mechanism was isolated and identified as being the kinetic effect associated with finite orbit widths [4].

That NTMs are so easily triggered by sawteeth at low beta in JET is due to the fact that ICRH dominant heating plasmas can produce very long sawteeth, and probably because in such conditions the toroidal plasma rotation is weak. Although unproven, it is probable that NTMs couple to the sawtooth precursor, and/or harmonics generated at the crash, more easily with weak rotation shear. This is clearly of great concern because ITER will operate with very low toroidal rotation velocity relative to the thermal velocity of the thermal ions, even during operation with full tangential NBI power. With this in mind it is important to explore ITER relevant sawtooth and NTM control experiments in JET. The experiments reported here are undertaken in the 'upgraded' JET with tungsten/beryllium wall, thus operating in conditions which have to contend with potential tungsten accumulation in the core. The experiments employ for the first time in JET a hydrogen minority heating scheme (in majority deuterium) with first harmonic ICRH resonance on the low field side (LFS), close to the $q = 1$

*See the Appendix of F. Romanelli et al., Proceedings of the 24th IAEA Fusion Energy Conference 2012, San Diego, US

surface on the outer mid-plane. Low field side resonance was employed many years ago in JET [5], but at high minority concentration (10-30 percent, thus operating in the margins of mode conversion), and more recently second harmonic was used to control sawteeth and avoid NTMs [6] . Such high concentration does not make for efficient ICRH, and in addition we have shown that sawtooth control is highly efficient when the concentration is low [3]. Employing LFS resonance is particularly ITER relevant because the ICRH antenna design of ITER does not allow for high field side resonance at full magnetic field. Recent JET experiments reported in Refs. [2, 3] employed high field side (HFS) resonance, and it was found that very close alignment of the RF resonance position and the inversion radius was required, and in addition care needed to be taken with the choice of phasing of the antenna. In contrast, the new experiments reported here investigate to what extent sawteeth can be controlled with (1) less accurate alignment of the ICRH resonance and (2) with various antenna phasings including dipole. The first point here is important if sawtooth control can be achieved routinely without complex control algorithms such as are employed with real time control techniques [7]. The second point is important because sawtooth control on the high field side relies on phased (-90^o) ICRH waves, which, relative to dipole phasing, has enhanced plasma-wall interaction via radio frequency-sheath redistribution effects [8]. ITER dedicated simulations [9] of ICRH and internal kink stability with fast ion effects have shown that in contrast to HFS experiments, LFS resonance should provide control with either $+90^o$ or -90^o phasing. The fast ion populations modelled are first harmonic ICRH minority ions, and neutral beam injected ions without second harmonic acceleration. The experiments reported here investigate this lack of sensitivity to the direction of the phasing, which clearly indicate that dipole waves should also provide access to control.

In addition to the avoidance of NTMs at low beta, frequent sawteeth have the advantage that impurities are flushed more regularly from the core of the plasma. While avoiding core impurity build up in an ITER fusion plasma is crucial, it is also very important in JET with the ITER-like wall, where radiative collapse or disruption sometimes occur, in part, when ELMs do not redistribute impurities sufficiently regularly and efficiently towards the edge. In addition, large intermittent ELMs are a source of impurities. Probably in line with localised electron cyclotron heating in ASDEX-Upgrade [10], it has recently been shown in JET [11] that centrally deposited ICRH can significantly enhance the plasma beta in the core, improve the general confinement, and reduce the central peaking of the tungsten impurities. In the experiments reported here, we show to what extent the core is flushed of impurities when using ICRH on the LFS just inside the $q = 1$ surface. Of particular interest is to see whether impurities that are flushed out of the core by the sawtooth crash are inhibited from returning inside $q = 1$ because of the localised electron temperature gradient produced close to the the ICRH resonance location. Without this effective impurity barrier, impurities can return easily to the core during the sawtooth ramping phase. Clearly, ideally, $q = 1$ localised ICRH would simultaneously shorten sawteeth (and thus avoid NTMs) and prevent impurity build up in the $q < 1$ region.

The paper is organised as follows. In section II the LFS ICRH experimental configuration is described, and low power L-mode experimental discharges are shown for conditions where short sawteeth are obtained, and where long sawteeth trigger NTMs and mode locking. Section III examines the mechanism responsible for the control of sawteeth in these experiments. The effect of ICRH antenna phasing on sawtooth period is explored in the experiments and with simulations of the ICRH heating [12–14]. The ICRH distributions are used to estimate the ICRH current drive and corresponding magnetic shear, and the effect of fast ions on the internal kink stability. In particular the HAGIS [15] code calculates the kinetic effects described in Refs. [2–4], which for this application, are the stabilising effects from NBI and ICRH trapped ions, and the potentially destabilising effects of asymmetrically distributed passing ions with finite orbit widths. Section IV explores high performance discharges in JET employing up to 19MW of NBI heating in conjunction with up to 5MW of LFS resonant ICRH with dipole phasing. The control of sawteeth in conjunction with impurity flushing is examined by moving the resonance through the $q = 1$ surface. The sawtooth impurity flushing is compared with full Lorenz orbit test particle simulations [16] in the evolving electromagnetic fields associated with Kadomtsev [17] reconnection. Conclusions are drawn in section V.

II. SAWTOOTH CONTROL WITH RESONANCE ON THE LOW FIELD SIDE

The experimental pulses described in this paper follow the approach of Refs. [2, 3] by sweeping the ICRH resonance across the $q = 1$ surface, usually from outside the $q = 1$ minor radius, to inside it. The difference from Refs. [2, 3] is that this is done for the first time on the LFS, with fundamental resonance, and with minority hydrogen in majority deuterium (concentration around 3 to 5 percent), as opposed to ^3He minority with HFS resonance. Fundamental resonance at frequency 37MHz was employed for all the L-mode pulses of this section. The configuration used in this paper is shown in Fig. 1, for the specific case of pulse 84500 at 15s in Fig. 2. The resonance position is swept through the $q = 1$ surface, as indicated in Fig. 2, by ramping magnetic field linearly from $2.72T$ to $2.36T$. The q profile is maintained as constant as possible by ramping the toroidal current proportionally from $2.4MA$ to $2.07MA$, with $q_{95} = 3.45$ and the sawtooth inversion major radius at around $R_{inv} \approx 3.28m$. For the HFS pulses of Refs. [2, 3] it was shown that sawteeth could be controlled (shortened) by using -90^o phasing over a narrow variation of the resonance position of about 3 or 4 percent of the plasma radius (about 3 or 4 centimetres). Figure 2 essentially extends Fig. 1 of Ref. [2] by again using -90^o phasing, but sweeping this time the resonance position through $q = 1$ on the LFS. Once again, this ICRH resonance sweep is undertaken with a pre-existing NBI power of nearly 3MW, which lengthens the sawtooth period to about 300ms. It is seen that short sawteeth are obtained over a much wider range of the sweep, in this case around 20 percent of the plasma

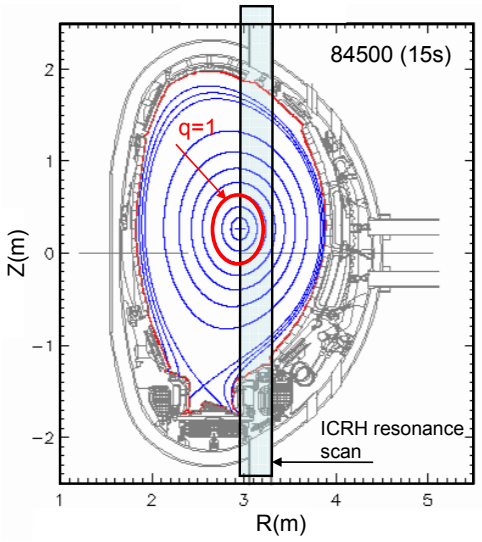

FIG. 1: Showing the configuration of JET pulse 84500 at 15s (similar for all the pulses shown in this paper). The red curve indicates the $q = 1$ surface, and the shaded box indicates the region over which the ICRH resonance is scanned over the pulse.

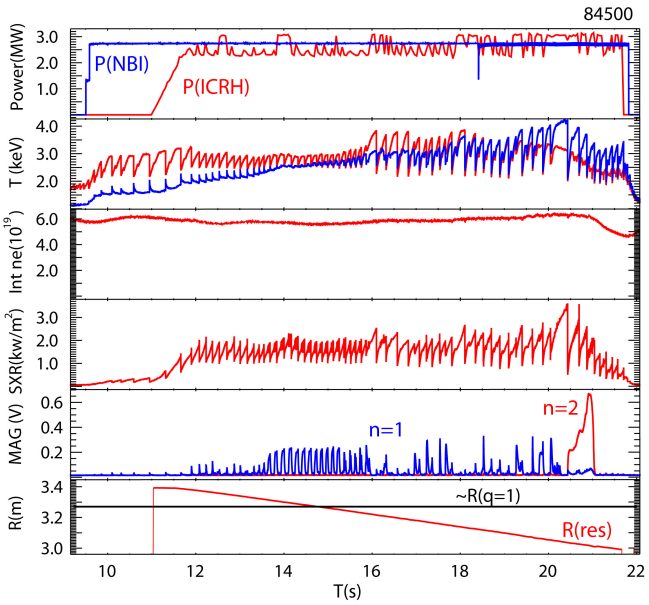

FIG. 2: Showing JET pulse 84500 which employed -90^o phasing ICRH of around 3MW, and 2.8MW of NBI, during a sweep in the toroidal field and toroidal current. Also shown are two (moving) ECE channels giving the temperature (the red T_e trace begins on the magnetic axis and ends off-axis, and the blue T_e trace begins off-axis and end on-axis), the line averaged density, a vertical core aligned soft x-ray channel, magnetic signals associated with $n = 1$ and $n = 2$ modes, the ICRH resonance position and an indication of the $q = 1$ position. The toroidal magnetic field was ramped linearly down from $2.72T$ to $2.36T$, and in proportion the toroidal current was ramped from $2.4MA$ to $2.07MA$.

radius, which is clearly an advantage over the HFS configuration of Refs. [2, 3]. We now examine what happens when sawteeth are not controlled: as the resonance position approaches the magnetic axis, an $n = 2$ tearing mode is triggered, and then locks (hence the vanishing $n = 2$ magnetics signal in Fig. 2). The mode causes reduction in plasma performance, though the plasma recovers after the auxiliary power is switched off. The mode was triggered at 20.4s by an uncontrolled long sawtooth of $450ms$, and at that moment the normalised beta was only $\beta_N = 0.5$, which is more than three times lower than the standard baseline scenarios envisaged for ITER [1]. The L-mode sawtoothing pulses described in this section and in Section III employ more ICRH power than NBI power, and as such the toroidal rotation velocity is weak. This could explain why NTMs are triggered so easily, and this in turn implies that sawtooth control should be taken seriously in ITER plasmas where toroidal rotation will be relatively weak compared to present day tokamak plasmas.

It is perhaps surprising that -90^o phasing is effective for sawtooth control on the LFS. The result is contrary to the LFS experiments of Bhatnagar *et al* [5] which showed that the Fisch [18] currents associated with -90^o phasing on the LFS should reduce the magnetic shear, and hence lengthen the sawtooth period, which indeed was observed. However, while Bhatnagar *et al* [5] operated at very high H concentration, our experiments operate at much lower concentration, where Fisch currents are weaker, and the hydrogen minority ions are more energetic. As a result the fast ion orbit width effects described in Refs. [2, 4] can be expected to be the dominant mechanism for sawtooth control providing that the fast ion distribution is asymmetric in the parallel velocity. As will be seen in the modelling shown in next section, the fast ion distribution functions, and in particular the asymmetry of the distribution functions, are quite similar for $+90^o$ and -90^o phasing (at this low level of minority concentration). The asymmetries (which can be measured e.g. by the fast ion current density) are caused by the same finite orbit width and detrapping processes for both phasings, and point to the possibility that dipole phased ICRH waves may produce similar fast ion distributions. This is indeed verified in the modelling shown in the next section, together with the new result that dipole phasing can also be used to control sawteeth. This last latter result is demonstrated empirically in Fig. 3 which shows two pulses where dipole ICRH is employed at about 2.5 MW in the absence of NBI. These pulses form the most basic sawtooth control configuration possible on JET. The pulses differ in that the large sweeps in the toroidal field, toroidal current and thus the resonance position, are in exact opposite directions. It is seen that in both cases sawteeth that are shorter than those during the Ohmic phase are obtained when the resonance position is close the inversion radius. The centre of this zone of control appears to correspond to resonance (major) radius slightly outside the inversion (major) radius. It is noted that in pulse 85932, the line integrated density was not controlled at the same level as 85930. The enhanced density led to the reduced temperature observable in Fig. 3. Nevertheless, the characteristics of the sawteeth did not appear to be significantly affected, and in particular,

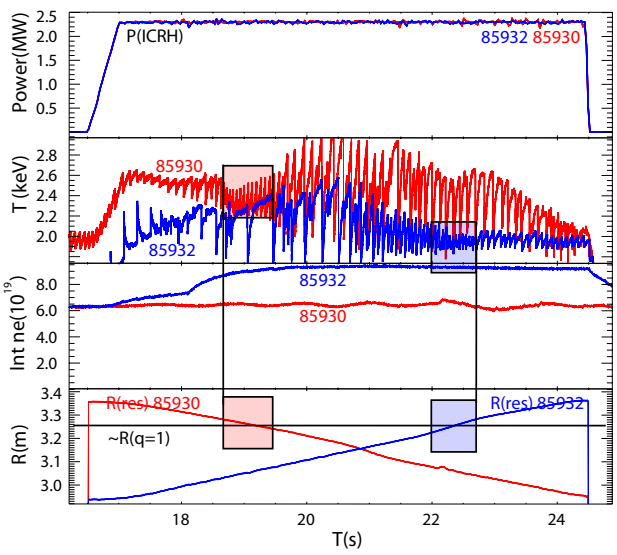

FIG. 3: Showing two JET pulses employing dipole phased ICRH, and no NBI power. Pulse 85930 (red) ramped the toroidal magnetic field and toroidal current respectively down from $2.7T$ to $2.33T$, and from $2.4MA$ to $2.1A$. Pulse 85932 ramped in the exact opposite direction. The plot shows identical ICRH power, an ECE channel measuring the central temperature midway through the pulses (about 21s), the line integrated density and the resonance positions relative to an approximate position of the measured inversion radius. Small sawteeth and corresponding resonance positions are indicated in shaded boxes.

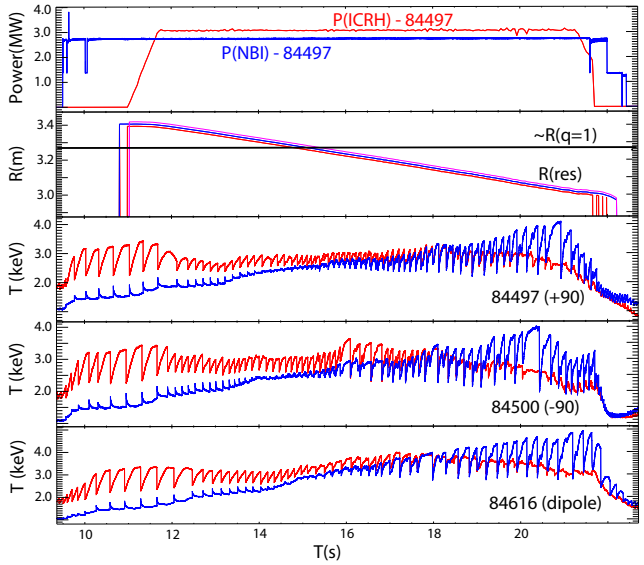

FIG. 4: Showing three otherwise similar JET pulses: 84497 employs $+90^o$ phasing, 84500 employs -90^o phasing, and 84616 employs dipole phasing. Each of the pulses commence with almost 3MW of centrally deposited NBI, and then 3.2MW or ICRH is applied during ramps in the toroidal magnetic field from $2.72T$ to $2.36T$, and in the toroidal current from $2.4MA$ to $2.07MA$.

any hysteresis observable in Fig. 3 is weak.

III. ISOLATION OF THE MECHANISM OF SAWTOOTH CONTROL

We have now seen that sawteeth can be controlled with -90^o phasing on the LFS, which is contrary to the results of Ref. [5] which employed high concentration hydrogen. It is clearly of interest to compare the effect of antenna phasing on sawtooth control, and also to model the equilibrium hydrogen minority fast ion population and the stability of the internal kink mode in order to isolate the mechanism for sawtooth control, and thus to understand the empirical results. Figure 4 shows three discharges which differ only in the antenna phasing. One of the pulses, pulse 84500 is the -90^o phased pulse also of Fig. 2, pulse 84497 employs $+90^o$ phasing, and 84616 employs dipole phasing. The pulses commence with nearly 3MW of NBI which lengthen the sawteeth to about $300ms$. As described earlier for Fig. 2, the toroidal field and toroidal current are ramped on application of about 3MW of ICRH, so that the RF resonance position moves from outside to inside $q = 1$. Each of the pulses triggered NTMs by the longest saweeth near the end of the heating phase despite each having normalised beta $\beta_N \approx 0.5$. In pulse 84497, the $n = 2$ mode locked, as indicated in Fig. 2, caused early rampdown of the ICRH, and a step down in the NBI. The effect of the resonance position sweep on the sawteeth can be compared across the three phasings. It is seen that the effect on the sawteeth is similar regardless of the phasing, though the effect appears to be slightly stronger for $+90^o$ phasing: the window of short sawteeth is widest, and at around $15s$ the sawteeth are shorter than any of the sawteeth in the other two pulses. These observations, together with the surprising finding that the window for short sawteeth is quite wide for all phasings, will be investigated in this section.

In order to model the effect of ICRH on the stability of the internal kink mode, the equilibrium fast ion distribution function f_h of the minority hydrogen ions needs first to be established. This has been undertaken with the codes, SELFO [12], EVE [13] and SCENIC [14], each having their own advantages and deficiencies. Figure 5 compares the energy density $(2\pi)^{-1} \int d\theta\, d^3v\, f_h m_h v^2/2$ obtained for these three codes at $15.2s$ in the -90^o phasing pulse 84497. The off-axis peak in each approximately coincides with the position of the resonance mapped on to the normalised minor radius ρ (where $\rho = 1$ marks the plasma edge). Agreement between the codes for this particular velocity moment is reasonably good, and it will be seen that the stability properties, which depend on the full phase space properties associated with the distribution functions, also agree quite well across the codes.

The stability associated with the energetic ions can be established via hybrid kinetic-MHD. The ideal internal kink mode, in the absence of two-fluid effects and resistivity (but including collisionless fast ion effects) is unstable for

$$\delta\hat{W} < 0, \tag{1}$$

where the ideal growth rate normalised to the Alfvén fre-

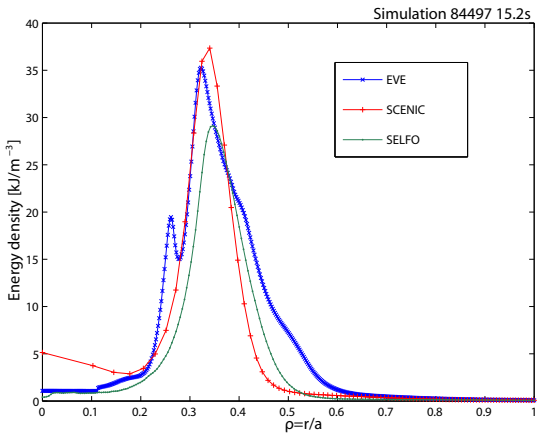

FIG. 5: Comparing calculations of the energy density from the three codes EVE, SELFO and SCENIC for the $+90^o$ pulse 84497 at 15.2s.

quency $\gamma_I/\omega_A = -\pi\delta\hat{W}/s_1$ with s_1 the magnetic shear at the $q = 1$ surface, and $\delta\hat{W} = \delta W/(2\pi^2\xi_r^2 R_0 B_0^2\epsilon_1^2)$. Here ϵ_1 is the local inverse aspect ratio at the $q = 1$ surface, B_0 and R_0 are the magnetic field and major radius at the magnetic axis, and ξ_r is the leading order radial eigenfunction at the magnetic axis for the $m = n = 1$ mode. For certain conditions it has been argued that resistive two fluid effects provide a stabilising effect, so that the ideal growth rate γ_I needs to be larger for instability, and thus δW should be more negative. In this case, the instability condition can be written [19]

$$s_c < s_1 \quad \text{where} \quad s_c = C\delta\hat{W} \tag{2}$$

where C is a positive definite constant, the magnitude of which does not matter for what follows. We are clearly interested in what impact the ICRH ions will have on the internal kink stability criterion. One way in which the ICRH ions can modify Eq. (2) is through modifying s_1. A particular feature of high energy ICRH ion populations, generated by minority heating, is that they form a fairly strong local current perturbation, which if positioned correctly, can affect s_1 [20]. For ICRH ions to control sawteeth via this 'shear mechanism' we would expect the magnetic shear at $q = 1$ to be enhanced by the ICRH ions for all three phasings at e.g. $15s$ for the pulses in Fig. 4. Modelling of the current produced by ICRH, including the plasma drag [5, 20], has been undertaken for these pulses at $15.2s$, and is shown in Fig. 6. The dipole structure of these currents is similar for all three phasings, although the current is strongest and most localised for the $+90^o$ case. The fast ion induced current introduces changes to the equilibrium q profile, which we model by adding the fast ion current density to the initial current density (common to all three pulses) in the absence of fast ion current, and then recalculate the toroidal equilibrium. Crucially, it is seen that these fast ion currents actually reduce the magnetic shear in the vicinity of the $q = 1$ surface, relative to the magnetic shear obtained in the equilibrium reconstruction obtained in the absence of the effect of the fast ions. It is thus seen that the 'shear mechanism' that has previously been used to interpret

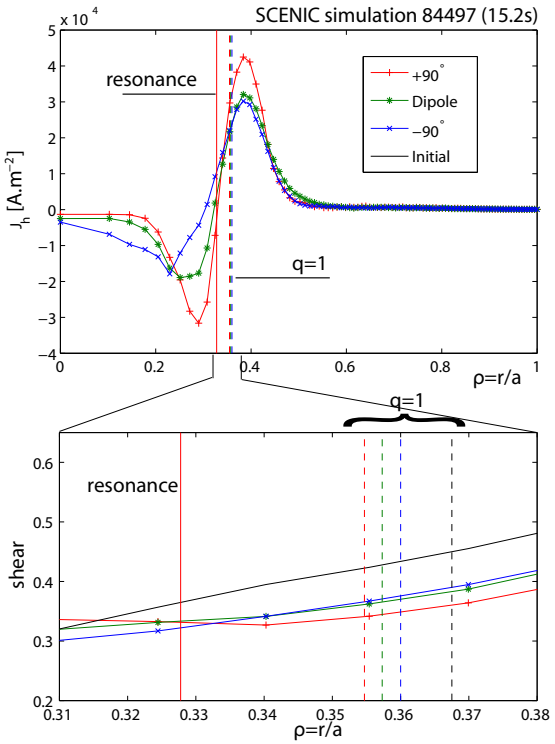

FIG. 6: SCENIC calculations of the ICRH contribution to the current density and corresponding magnetic shear for pulses 84497 ($+90^o$), 84500 (-90^o) and 84616 (dipole) each at 15.2s. All take into account the plasma drag current [5, 20]. The shear profile in the absence of the fast ion currents is also shown.

[5, 20] sawtooth control certainly cannot hold for the minority ion experiments reported here. According to Eq. (2) the shear effect is actually stabilising to the internal kink mode, and thus the present experiments are even more contrary to the 'shear mechanism' of sawtooth control than the HFS experiments using ^{3}He minority in Ref. [3]. The latter experiments were designed to have vanishing shear perturbation from the fast ions. The present experiments, and the experiments of Ref. [2, 3] can instead be understood through the effect of the fast ions on δW. We expect that where sawteeth are controlled, the ICRH ions will produce a strongly negative contribution to $\delta\hat{W}$, which if sufficiently large in amplitude (compared to contributions to δW from the bulk plasma and the NBI ions), would satisfy both the ideal instability criterion of Eq. (1) and the resistive two-fluid instability criterion of Eq. (2).

The hot ion contribution to δW is (Ref. [2] and references therein):

$$\delta W_h = -\frac{1}{2}\int d^3x\, \boldsymbol{\xi}^* \cdot \boldsymbol{\mathcal{F}}_h,$$

where $\boldsymbol{\xi}^*$ is the complex conjugate of the plasma displacement $\boldsymbol{\xi}$. The perturbed force

$$\boldsymbol{\mathcal{F}}_h = -\boldsymbol{\nabla}\cdot\underline{\underline{\delta P_h}}.$$

is thus seen to depend on the hot ion contribution to

the pressure tensor $\underline{\underline{\delta P_h}}$, which is obtained by taking moments of the solution δf_h of the drift kinetic equation, i.e. the Vlasov equation in reduced phase space. The perturbation of the distribution function about the equilibrium distribution f_h can be written [21] in terms of perturbations of the three quantities that are conserved in the equilibrium state:

$$\delta f_h = -\delta P_\phi \frac{\partial f_h}{\partial P_\phi} - \delta\mu \frac{\partial f_h}{\partial \mu} - \delta\mathcal{E} \frac{\partial f_h}{\partial \mathcal{E}}, \qquad (3)$$

where P_ϕ is the toroidal canonical momentum, $\mathcal{E}$ is the kinetic energy of a particle, and μ is the magnetic moment. Figure 7 plots the $\delta\hat{W}$ contributions associated with the ICRH distribution function and the NBI distribution function for the $+90^o$ pulse 84497 at $15.2s$. In this plot the MHD contribution to δW is evaluated with the MISHKA code [22], and the fast ion contributions are evaluated with HAGIS [15]. The latter code takes distributions from both SCENIC [14] and SELFO [12], and the eigenfunctions from MISHKA for varying $q = 1$ radius r_1. In HAGIS the mode frequency and growth rate is taken to be zero, and the imaginary part of δW is neglected. The plots are shown as a function of the difference between the resonance location and the $q = 1$ radius, and thus reflects the evolution of the pulse where the resonance position is swept through $q = 1$ from outside to inside. The δW contributions from SCENIC and SELFO compare well, with both showing a deep minimum in δW when the resonance position is aligned with or just outside $q = 1$. The strong destabilising contribution from ICRH is contrasted with the weak destabilising effect from MHD, and the strong stabilising effect from NBI, where the NBI ion distribution has been obtained from the TRANSP [23] code. The NBI and MHD contributions vary in the plot because of their dependence on the $q = 1$ radius, though it is seen that this dependence is weak compared to that of the ICRH distribution.

As discussed in Refs. [2–4], the reason for the strong minimum in δW as the RF position passes close to the $q = 1$ surface has to do with the asymmetry in $v_\parallel$ of the equilibrium ICRH fast ion distribution function, and in particular its radial variation. Passing ions with large radial drift excursion that intersect the $q = 1$ surface strongly affect stability. A net effect from a population occurs if the number of co and counter passing ions is not balanced, especially when the ratio of co and counter passing ions varies through the $q = 1$ surface. A measure of the latter is the radial gradient of the current associated with the fast ions dJ_h/dr where $J_h = eZ_h \int d^3v\, v_\parallel f_h$ and f_h is the fast ion distribution function associated with ICRH (without the plasma drag current subtracted), evaluated for example by SCENIC. In Ref. [4] it was shown that for the ICRH population, with resonance close to the $q = 1$ surface,

$$\delta W_h \propto -\frac{d}{dr} J_h(passing).$$

We can visualise the radial variation of the distribution function, and thus understand the trend in δW exhibited in Fig. 7 by inspecting Fig. 8. The parallel current profile generated by passing ions (without the drag current subtracted) is shown for the dipole pulses 84616 at 15.2s, and three positions are indicated in the profile: one at the minimum in J_h (line (a)), one at the resonance position where the current is small, (line (b)), and one at the peak in the current (line c). Also shown are contours of the distribution function from SCENIC labelled (a), (b) and (c) according to the positions indicated in the current profile, plotted as a function of $v_\parallel$ and $v_\perp$ on the outboard midplane at these three radial positions. Both passing and trapped fractions (the trapped-passing boundary is indicated by the straight white lines) are shown to be asymmetric in $v_\parallel$ at the radial locations of the peak and trough of J_h.

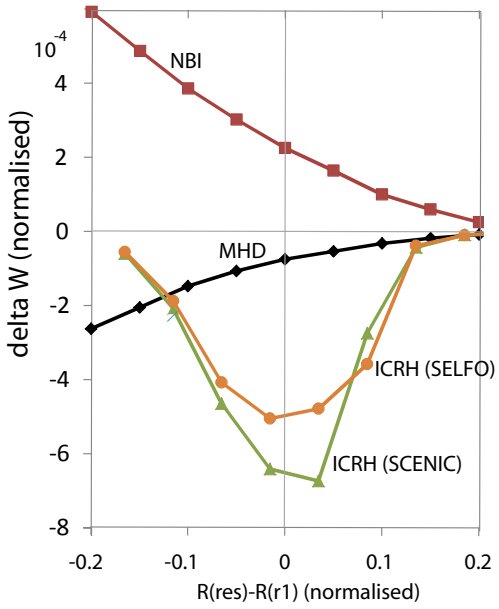

FIG. 7: HAGIS simulation of $\delta\hat{W}$ for $+90^o$ pulse 84497, plotted as a function of normalised resonance position relative to $q = 1$ radius $(R(res) - R(q = 1))/(R(r = a) - R_0)$. Also shown is the stabilising contribution from NBI ions, and destabilising MHD contribution. ICRH markers are taken from both SELFO and SCENIC.

Figure 9 compares the total δW, including the effects of ICRH ions, NBI ions and MHD, with the sawtooth period measured for the three pulses of Fig. 9. All are plotted with respect to $(R(res) - R(q = 1))/(R(r = a) - R_0) \approx [r(res) - r_1]/a$ with a the plasma minor radius. Note that $R(r = a) - R_0$ is about $88cm$, and for the experimental data, the $q = 1$ radius is measured by the inversion radius for each sawtooth event. The ICRH distribution functions for the three phasings were evaluated with the SCENIC code. The general trends of the simulations are in reasonable agreement with the experimental data. For example the strongest destabilisation occurs for $+90^o$ phasing, and the weakest for dipole phasing. All cases show a region of destabilisation (short sawteeth, or negative δW) which are centred about a value of resonance position $R(res)$ a few centimetres outside the $q = 1$ radius. In addition the region of destabilisation extends to more negative values of $R(res) - R(q = 1)$ for $+90^o$ phasing.

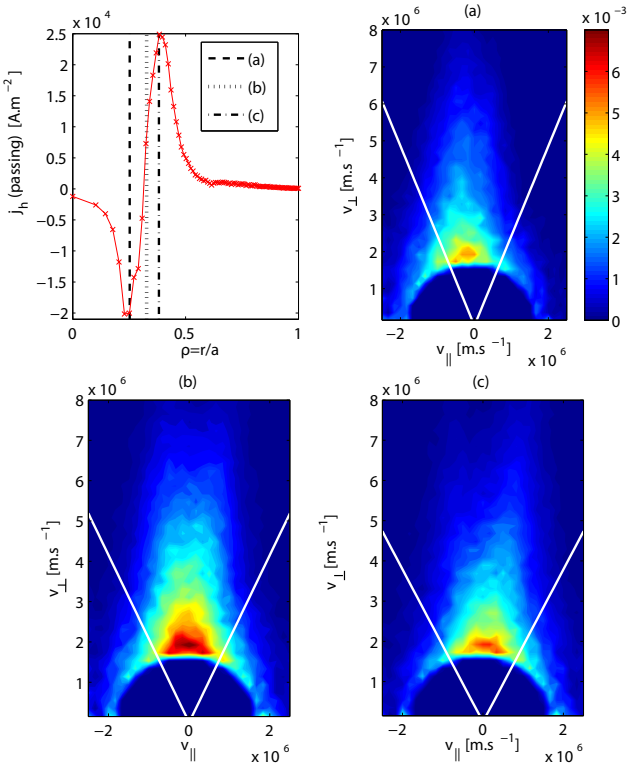

FIG. 8: Fast passing ion current $J_h(passing)$ for dipole pulse 84616 at 15.2s and marked positions for contour plots of the distribution function from the SCENIC code. Distribution function plots undertaken on the outboard midplane show parallel velocity asymmeties are consistent with expectation from the local sign and amplitude of the current.

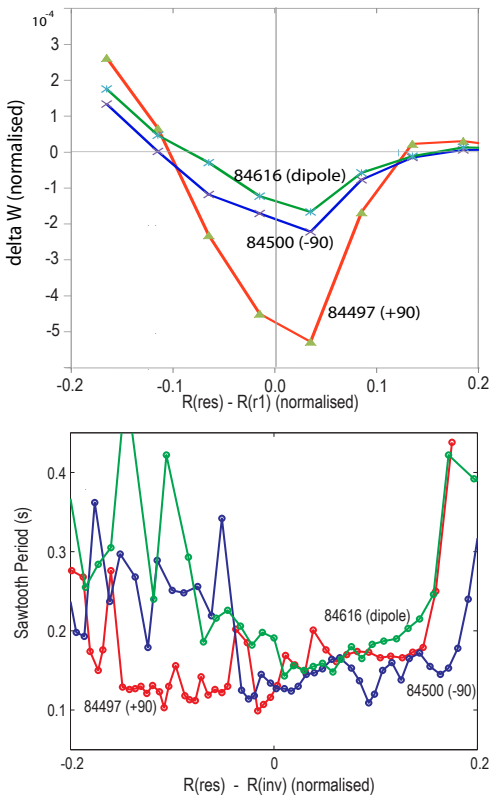

FIG. 9: Showing simulations of the total δW as a function of $(R(res)-R(q=1))/(R(r=a)-R_0)$ for the three pulses 84497 $(+90^o)$, 84500 (-90^o) and 84616 (dipole). These results are compared with experimental deduction of the sawtooth period, plotted as a function of the $(R(res)-R(q=1))/(R(r=a)-R_0)$ where $R(q=1)$ is measured by the inversion radius for each sawtooth event.

IV. SAWTOOTH CONTROL AND IMPURITY FLUSHING DURING HIGHER PERFORMANCE PULSES

The applicability of ICRH control of sawteeth on the low field side is routinely effective during L-mode plasmas at JET. However, H-mode plasmas with the new all-metal wall encompass new challenges that have to be handled at the same time as the sawtooth control. In order to prevent impurities from penetrating the core plasma, and to avoid radiative collapse, the ELM frequency has to be sufficiently large soon after H-mode generation, and during the rest of the pulse. In the plasmas described here, the ELM frequency was maintained at about 25Hz by using a novel technique involving realtime dosing of the plasma [24]. The fuelling is increased in realtime if an ELM is not detected quickly enough after the previous ELM, or fueling is reduced if the next ELM comes too soon [24]. Figure 10 shows regular ELMs in pulse 85080 where this active ELM feedback was undertaken. The central SXR signal indicates nevertheless that impurities accumulate steadily in the plasma core within about two seconds after application of the heating. In this pulse the NBI power was held reasonably constant at about 19MW, while dipole phased ICRH of 5MW was swept through the $q=1$ surface from outside to inside. When the resonance position passed a few centimetres inside the measured inversion radius the SXR signal reduced to the extent that a few consecutive sawteeth could barely be seen through variation of the central SXR channel displayed in Fig. 10. This pulse, and all the other H-mode pulses referred to in this section employed dipole phasing using fundamental resonance with frequency 42MHz. In 85080, the magnetic field was ramped down from $3.1T$ to $2.7T$. The q profile is maintained constant by ramping the toroidal current proportionally from $2.8MA$ to $2.45MA$, with $q_{95}=3.45$.

In Fig. 10 it is seen that the addition of 5MW of ICRH power to the pre-existing NBI power was offset by an enhancement to the radiative power of almost the same amount. The virtues of ICRH are observed as the resonance passes inside $q=1$ when the central temperature increases by almost 20 percent over one sawtooth cycle. This is particularly evident in Fig. 11 (f) where temperature profiles for 85080 are plotted just before the sawtooth crash at 12.04s (a) and just before the consecutive sawtooth crash at 12.43s (e). Figure 11 also shows radiative power tomography [25], just before (a) and just after (b) to the sawtooth crash at 12.04s, as well as just before the next crash at 12.43s. The extremely peaked

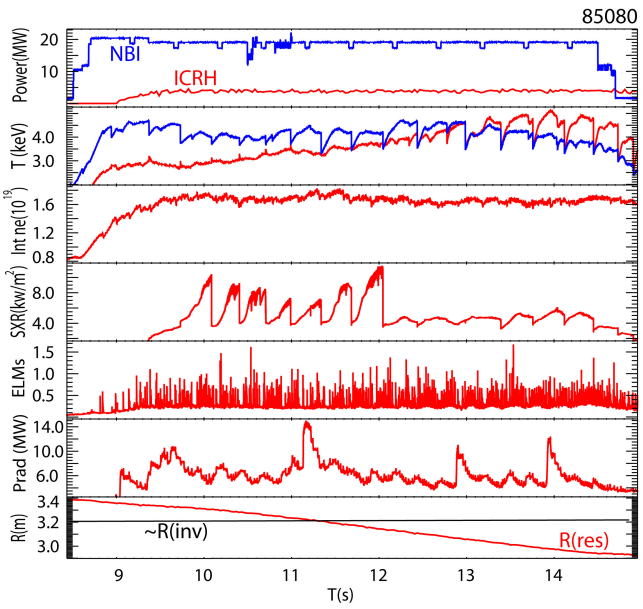

FIG. 10: Showing high performance H-mode pulse 85080, by plotting NBI and ICRH power, central electron temperature, line integrated density, central SXR, ELM fluctuations, radiation power, and ICRH resonance position relative to $q = 1$.

impurity population, clearly visible just prior to 12.04s, is redistributed outside $q = 1$ by the sawtooth event, in agreement with recent 3d sawtooth cycle simulations [26]. The ICRH resonance position being a few centimetres inside $q = 1$ appears to prevent the impurities from re-entering the core; influx during the sawtooth ramp would ordinarily be expected to occur. It is assumed that the strong temperature gradient near $q = 1$ due to the local ICRH resonance introduces a strong inward impurity transport barrier [27]. It thus seen that a combination of sawtooth reconnection and localised thermal gradients is particularly effective, where the former ejects particles almost instantaneously (but intermittently), and the latter reduces the inward transport of impurities over the sawtooth quiescent phase. As seen in Fig. 10, when the resonance position moves close to the magnetic axis near the end of the pulse, the SXR signal grows again, partly because the slightly increased central temperature naturally enhances the central SXR signal, but also possibly because impurities are once again able to penetrate the $q = 1$ surface and reach the core during the sawtooth ramp phase.

The outward motion of impurity ions during the sawtooth crash has been modelled using the EBdyna_go code [16], which accounts for the full Lorenz motion of test particles in evolving electromagnetic fields. These fields are derived from the Kadomtsev model, and it is found that the particles drift outwards during the crash, as shown in Fig. 11 for the simulations of pulse 85080 just before (c) and after (d) the sawtooth crash at 12.04s. The code does not model the enhanced anomalous transport due to strong temperature gradients [27], nor does it include centrifugal effects on the massive toroidally rotating tungsten ions, which are clearly visible in the experimental data via the enhanced SXR signals on the

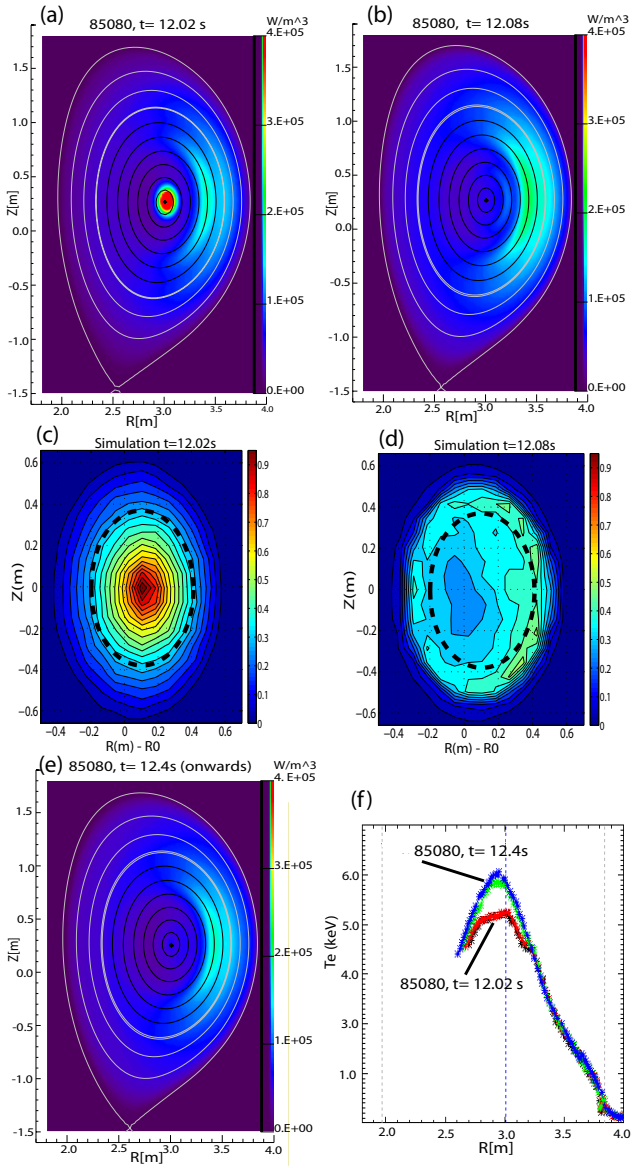

FIG. 11: Showing radiative power tomography from 85080, before (a) and after (b) the sawtooth crash at 12.04s. These can be compared with simulations of impurity density at the same times (c) and (d). Also shown (e) is SXR tomography just prior to the next sawtooth crash at 12.43s. The electron temperature profile is plotted in (f) at times just before the consecutive sawtooth crashes at 12.04s and 12.43s. The $q = 1$ surface lies just inside the cenfrifugally peaked impurities on the low field side, and runs along the nearest black contour in the tomography figures of (a), (b) and (e).

outboard midplane at all times.

The question still to be answered is whether experiments can be constructed that prevent both density accumulation during the sawtooth ramping phase, and control the sawteeth in order to avoid unwanted secondary MHD events like NTMs, which can also further increase impurity fluxes to the core. It appears that this ought to be possible because the L-mode pulses of the previous section showed that the sawteeth can be controlled with

the resonance position just inside $q = 1$, which we have seen is good location for preventing impurity build up. This was achieved in for pulse 85082, shown in Fig. 12, by starting with the resonance closer to $q = 1$ (than in 85080), and slowing the ramp in the toroidal magnetic field and the toroidal current. As the resonance moves inside $q = 1$ it is seen that the central SXR strongly reduces (though for unknown reasons not as strongly as in 85080), and two consecutive moderately shorter sawteeth are produced. It appears that in order to trigger short sawteeth in these high power pulses the resonance position has be more accurately placed than for the L-mode pulses described earlier. This is likely to be due to the fact that relative to the NBI power, the ICRH power is much lower in these high performance pulses, and also that the effects of impurity accumulation, and its dependence on both sawteeth and ICRH resonance position, clouds the ICRH sawtooth control mechanism described in the previous section. Nevertheless a statistical examination of eight consecutive high power pulses shows that sawteeth were controlled over a narrow range of resonance radius $R(res)$. Figure 13 indicates that the sawtooth period was reduced by about 30 percent, with the optimal resonance position being about 6 centimetres inside the inversion radius $R(inv)$, a position which appears also to be favourable for keeping impurities outside the $q = 1$ surface, and thus reducing core radiation. Efforts also continue to fine tune the resonance position, and to enhance the ICRH power, so that the sawteeth can be controlled as effectively as the L-mode pulses described earlier. It should be pointed out, however, that the pulses in Fig. 13 with the strongest effect of ICRH resonance position on the sawteeth were at the lowest NBI power (11-16MW) and lowest ICRH power (2-3.5MW). It has already been shown that sawtooth control works very successfully in low power L-mode, where in fact about 1MW of ICRH power is capable of controlling the sawteeth. But, sawtooth control with ICRH appears to become much more challenging deeply in H-mode, and it is not yet clear, especially e.g. from the trends seen in Fig. 13, whether ICRH power much larger than the maximum in Fig. 13 would provide, for example, a reduction of the sawteeth by much more than the maximum observed in Fig. 13, i.e. about 30 percent.

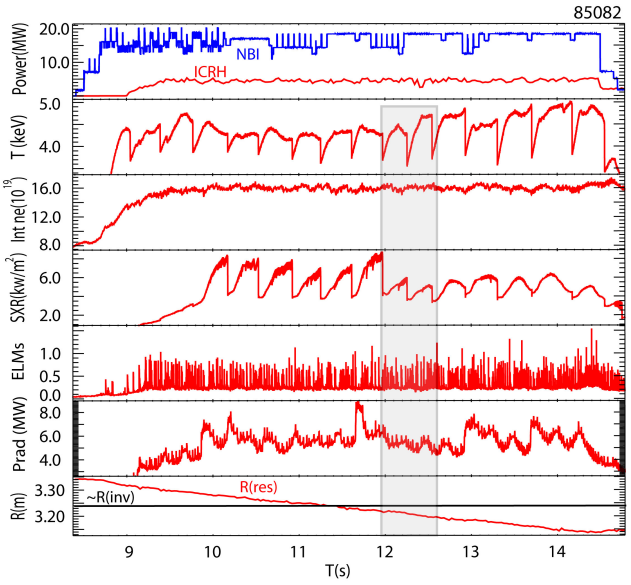

FIG. 12: Showing 85082, a similar pulse to 85080, Fig. 10, but with a slower ramp, so that sawteeth were controlled when the resonance passed a few centimetres inside $q = 1$, and impurities were flushed from the core.

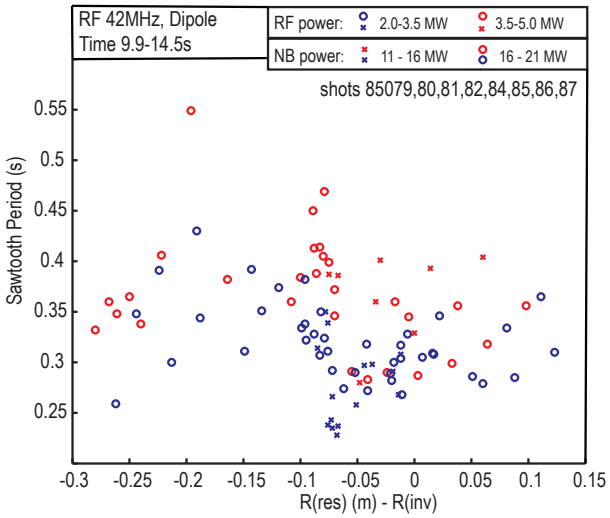

FIG. 13: Showing Sawtooth control over eight consecutive high power H-mode pulses. The sawtooth period is plotted as a function of $R(res) - R(inv)$ during the decreasing ramps in magnetic field $3.1T < Bt < 2.7T$, and reducing toroidal plasma current $2.8MA < Ip < 2.45MA$, with $q_{95} = 3.45$.

V. CONCLUSIONS

Sawtooth control experiments have been conducted for the first time at JET employing low concentration minority heating with fundamental resonance in the low field side (LFS). This ITER relevant configuration has been shown to be favourable compared to high field side (HFS) sawtooth control experiments in at least two respects. First, in L-mode plasmas, the resonance position does not have to be placed very accurately, which ultimately means that realtime movement of the resonance position is required less than for the HFS experiments reported in Refs. [2, 3]. Secondly, it is found that the sawteeth can be controlled with various ICRH antenna phasings, which in practice enables sawtooth control techniques to be adopted in high performance H-mode pulses, where dipole phasing is preferred (due to less plasma wall interaction by RF sheaths [8]) in order to best protect plasma facing components and the all-metal wall. When sawteeth were allowed to be long in these L-mode pulses, NTMs and locked modes were triggered by the long sawteeth at very low normalised beta, $\beta_N \approx 0.5$. This is three times lower than the normalised beta envisaged for baseline scenarios in ITER. Similarly to ITER plasmas, the L-mode plasmas reported here have low toroidal plasma flow shear, prime conditions for mode coupling across neighbouring rational surfaces.

Dedicated internal kink stability simulations of these experiments show that all phasings of the ICRH are effective for sawtooth control, although it is found that $+90^o$ phasing is the most efficient phasing, in agreement with experiment. These stability calculations take ICRH marker distributions from the SELFO and SCENIC codes, and it is once again [2, 3] found that fast ion orbit widths and parallel velocity asymmetry in the ion distribution function are probably responsible for the sawtooth control. In contrast, calculation of the fast ion driven current, indicates that when the ICRH resonance position is close to the $q = 1$ surface, the shear at $q = 1$ is actually reduced by the ICRH induced current for all phasings. This should be stabilising to the internal kink mode, which thus indicates that the traditional shear mechanism for sawtooth control [5, 20] is outweighed by the fast ion mechanism [2, 4], or perhaps some other mechanism that has not been discovered, nor the physics accounted for in simulations.

Sawteeth were routinely and easily controlled in L-mode plasmas, including plasmas near the L-H threshold, but achieving sawtooth control with ICRH in H-mode remains challenging. In order to produce frequent ELMs the redistribute impurities in the edge, and to avoid intermittent ELMs which sputter tungsten from the wall, H-mode plasmas employ high power NBI, typically more than 15MW, often in conjunction with real-time ELM control techniques [24]. This five fold increase in NBI power (compared to the L-mode plasmas reported here), dwarves the ICRH power coupled in these ELMy plasmas, and as a result the relative amplitude of the sawtooth control actuator is much reduced. Nevertheless this paper reports pulses where sawtooth control has been achieved in H-mode. It has been found that the resonance position must be closely constrained to be a few centimetres inside the inversion radius, and that this ICRH location comes with the crucial advantage that impurities displaced outside $q = 1$ during the sawtooth crash appear to reinvade the core at a much lower extent (between consecutive sawtooth crashes) than when the resonance position is outside $q = 1$. The creation of an inward impurity transport barrier near the $q = 1$ surface is suggested to be consistent with the establishment of a strong electron temperature gradient [27] near the local ICRH resonance. Clearly the barrier must be positioned inside the sawtooth inversion radius, with the optimal position intuitively being just inside the inversion radius. Future experiments will concentrate on increasing the relative amplitude of the ICRH power in order to control the sawteeth more efficiently in H-mode, while at the same time assessing the efficiency of the local ICRH resonance for creating an impurity barrier in the core, and for enhancing core temperature. In addition realtime sawtooth control techniques [7] will be developed in these LFS experiments. Such techniques will have the greatest application in H-mode pulses where the resonance position must be positioned accurately through the discharge.

Acknowledgements

This work, supported by the Swiss National Science Foundation, and by the European Communities under contract of Association between EURATOM and Confédération Suisse, was carried out within the framework of the European Fusion Development Agreement. The views and opinions expressed herein do not necessarily reflect those of the European Commission. SCENIC simulations were performed on BlueGene cluster at EPFL, Lausanne (CH), on ROSA XE6 cluster at CSCS, Manno (CH) and on Helios at CSC, Rokkasho (Japan)

[1] I. T. Chapman, *et al*, Nucl. Fusion **50**, 102001 (2010)
[2] J. P. Graves, *et al*, Nature Commun. **3**, 624 (2012)
[3] J. P. Graves, *et al*, Nucl. Fusion **50**, 052002 (2010)
[4] J. P. Graves, *et al*, Phys. Rev. Lett. **102**, 065005 (2009)
[5] V. P. Bhatnagar, *et al*, Nucl. Fusion **34**, 1579 (1994)
[6] O. Sauter, *et al*, Phys. Rev. Lett. **88**, 105001 (2002)
[7] M. Lennholm, *et. al.*, Nucl Fusion, **51**, 073032 (2011)
[8] A. Czarnecka, *et. al.*, Plasma Phys. Control. Fusion **53** 035009 (2011)
[9] I. T. Chapman, *et al*, Plasma Phys. Control. Fusion **53**, 124003 (2011)
[10] R. NEU, *et. al.*, Plasma Phys. Controlled Fusion **44**, 811 (2002).
[11] M. Goniche, *et al*, EPS proceedings 2014
[12] J. Hedin *et. al* Nucl. Fusion **42**, 527 (2002)
[13] R. Dumont and D. Zarzoso Nucl. Fusion **53**, 013002 (2013)
[14] M. Jucker, *et. al.*, Plasma Phys. Control. Fusion **53**, 054010 (2011)
[15] S. D. Pinches *et. al.* Comput. Phys. Commun. **111**, 133 (1998)
[16] F. Jaulmes *et al* "redistribution of fast ions during sawtooth reconnection," subm. Nucl. Fusion (2014)
[17] B. B. Kadomtsev, Sov. J. Plasma. Phys. **1**, 389 (1975)
[18] N. J. Fisch *et. al.* Rev. Mod. Phys. *59*, 175 (1987)
[19] F. Porcelli, *et al*, Plasma Phys. Control. Fusion **38** 2163 (1996)
[20] L.-G. Eriksson, *et al*, Nucl. Fusion **46**, S951 (2006)
[21] P. Helander, *et al*, Phys. Plasmas **4**, 2181 (1997)
[22] I. T. Chapman, *et al*, Phys. Plasmas **13** 062511 (2006)
[23] R. V. Budny, Nucl. Fusion **32**, 429 (1982)
[24] M. Lennhom, in preparatrion Plasma Phys. Control. Fusion (2014)
[25] T. Pütterich *et al*, Plasma Phys. Control. Fusion **55**, 124036 (2013)
[26] T. Nicolas, *et al*, Physics of Plasmas **21**, 012507 (2014)
[27] M. Valisa, *et al*, Nuc. Fusion **51**, 033002 (2011)